Peer-reviewed version available at Nanomaterials 2019, 9, 766; doi:10.3390/nano9050766

Article

Impact of nitrogen foamed stimulation fluids stabilized by nanoadditives on reservoir rocks of hydrocarbon deposits

KlaudiaWilk [1,*], Piotr Kasza [1], Krzysztof Labus[2]

[1] Oil and Gas Institute – National Research Institute; wilkk@inig.pl, kasza@inig.pl
[2] Silesian University of Technology; krzysztof.labus@polsl.pl
* Correspondence: wilkk@inig.pl; Tel.: +48134368941

Abstract: First objective of this experiment is to improve the stabilization of N_2 based foam with nanoparticles as an alternative to typical fracturing fluid which consists of a gelling agent (HPG). The second objective of the project is to investigate the damage caused by nanoparticle–based nitrogen foamed fracturing fluids (F.F) on a reference sandstone, using permeability and porosity tests, Optical Microscope with Profilometer and Scanning Electron Microscope (SEM). The properties of F.F with two types of SiO_2 nanoparticles (hydrophilic fumed silica Areosil 300 and silica sol U-2 obtained by sol-gel method), such as rheology and core damage were investigated. The discussion of this research results is based on the stability tests carried out with the use rheology and the foam half-life, formation damage ratio and observation of exposed samples using SEM and Profilometer. The permability and porosity damage ratios of the damaged core samples were found to decrease when nitrogen foamed fluids were used. These results were confirmed with Profilometer and SEM images. The experimental data showed that the foam stability increased when silica (SiO_2) nanoparticles were added. SiO_2 nanoparticle-surfactant-stabilized foam for fracturing is superior to traditional water-based fracturing fluids and causes lower core permeability damage than a traditional F.F.

Keywords: nanoaditives; nitrogen foamed stimulation fluids; reservoir stimulation; rheology; formation damage; SEM

1. Introduction

One of problems facing the oil industry is the production of as high as possible amounts of oil remaining in the reservoir after using up natural energy conditions. In many hydrocarbon reservoirs exploited worldwide the mining approaches the final phase [1]. By means of the first extraction methods utilising the reservoir energy it is possible to obtain only approx. 5–20% of resources [2,3]. Therefore for many oil companies the development of hydrocarbons stimulation methods is today a priority. Stimulation treatments such as HF [4], matrix acidizing, acid fracturing [5–7] or EOR [8–10] are common techniques used to increase the extraction productivity. In all aforementioned cases the stimulation (injection) fluid is a crucial element and must meet special requirements depending on the goal of application [11–13]. After stimulation treatments a part of this fluid remains within fractures causing damage to the formation and reducing the stimulation effectiveness [14–16]. Therefore attention has been drawn to the possibility of applying fluids energised with gases with the addition of nanoparticles, reducing thereby the water content in the injection fluid and also increasing the stabilisation of the process fluid during stimulation treatments [17–21]. The advantage of energised fluids consists also in increased fluid recovery after fracturing due to the natural energy of the gaseous fluid component [22,23]. Because the gas decompresses during the pressure reduction and fluid reception after the treatment, the dissolved gas helps to recover the pumped fluids and facilitates the well cleaning [24,25]. Moreover, high viscosity of the foam, allows better transport of

the proppant and more effective placing it in the fracture without excessive falling of the proppant material [26,27]. It ensures also good control of the fluid filtration to the rock matrix and to natural fractures during fracturing. Their application allows to reduce significantly the amount of water necessary for treatments [18,28,29], limiting the possibility of clayey minerals swelling in the deposit, causing reduced permeability [30,31]. In the case, when the fracturing fluids are made on the basis of water, so-called permeability damage can occur, caused by swelling of clayey minerals or action of other physical and chemical mechanisms proceeding in the fractured formation [32]. They reduce the reservoir rocks permeability at the stage of drilling, hydraulic fracturing, production, and other reservoir operations, resulting in decreased reservoir productivity [33], which translates directly into economic effectiveness.

The nanotechnology is a fast developing field offering a multitude of potential applications and benefits [34–37]. Nanoparticles feature a number of advantages during the reservoir stimulation with foamed fluids, such as: they can increase the foam stability [38], they are that small that can stabilise small bubbles, which increase viscosity - necessary for effective transfer of the proppant material [39], they are much smaller than rock fractures and pores [40], which allows more effective transport to the surface of the post-treatment fluid during the process of well cleaning, they reduce migration of solid particles [41], they are environment-friendly [42], and they can reduce corrosion. What is more important, the mechanism of nanoparticles movements and action [43–46], and also of foam stabilisation by nanoparticles differs and is more effective than that utilising surfactants and emulsifiers. After the stage of pumping and placing the proppant in the fracture, foam loses its stability and viscosity, and foam bubbles regenerate during the fluid recovery after the treatment [47].

2. Materials and Methods

Using the tap water as the base, a foamed stimulation fluid was formed by the addition of N_2, of a foamer, of nanoparticles, and of natural polymer. Silicon dioxide (U-2), in the form of 23% water solution, was the first type of used nanoparticles. The silica sol was obtained by the sol-gel method. Tetraethoxysilane (TEOS) was a direct substrate used to obtain the silica sol. The reaction was carried out in a water-alcohol medium at the presence of ammonia solution within a pH range of 10.97 to 11.00. The process was proceeding as follows: anhydrous ethanol, ammonia solution, and distilled water were mixed in an Erlenmayer flask using a mechanical mixer. pH of the formed solution was measured after 15 minutes. The pH value of reaction mixture prepared during the process of silica sol formation was strictly controlled to ensure repeatability of SiO_2 particles size. Then TEOS was added at continuous mixing. In the initial stage of synthesis the reaction mixture (sol) was clear, after a dozen or a few dozen minutes the solution opalescence was observed. The process was stopped after 3 hours of intensive mixing. Based on the photon correlation spectroscopy the sol particle size was found to be 30 nm. To obtain a 23% SiO_2 solution the obtained silica sol was concentrated through evaporation of solvents to a defined volume.

Silica nanoparticles (Areosil 300) was the second type, obtained from Evonik Industries. The colloidal silica, referred to as 'fumed silica', because it is produced through continuous flame hydrolysis, via combustion of silica tetracholoride $SiCl_4$ in an oxygen-rich flame. The silica powder features an extremely low density of 90 g/l and a high specific surface area of 300 m^2/g (+/- 30 m^2/g). Areosil 300 is a mixture of lipophobic and hydrophilic nanoparticles (LHP) with a mean particle size of approx. 7 nm. Its composition contains silicon dioxide (SiO_2) > 99.8%, aluminium oxide (Al_2O_3) < 0.05%, titanium dioxide (TiO_2) < 0.03%, hydrogen chloride HCl < 0.025%, and iron III oxide (Fe_2O_3) < 0.003%. pH ranged between 3.70 and 4.70. Initially, nanoparticles in the form of a powder (AEROSIL 300) or of a suspension (U-2) were added to the tap water at room temperature, then the solution was stirred with a mechanical mixer during 4–5 minutes. After that period the sample was subject to ultrasonic waves action using a homogeniser during 4 minutes, at an amplitude of 70%. Anionic foaming agent A from CESI Chemicals was added next (4 ml/l), and finally optionally polymer W (natural, fast hydrating guar gum for oil field applications) (made by Weatherford) was added at an amount of 1 g/l. Agents A and W were used based on our previous work to assess the best additives

Peer-reviewed version available at Nanomaterials 2019, 9, 766; doi:10.3390/nano9050766

to foamed fluids [48,49]. Samples of model rock material, taken from a depth of approx. 300 to 400 m, originating from a deposit situated in the upper part of Lower Istebna beds, were taken for laboratory tests to determine the degree of damage. These strata exist mainly in the form of thick-banked massive fine- and medium-grained sandstones with clayey-limy binder with subordinate shale banks. Beds of Inoceramian facies prevailing with shale exist both above and below those sandstones complexes.

2.1. Viscosity of the Stimulation Fluids

To prepare fracturing fluids with nanoparticles addition, to carry out rheological measurements, the procedure described in sub-section 2 *Materials and Methods* was followed. The fluid was then introduced to tubes of a pipe rheometer designed specifically to measure the rheological properties of foamed systems under extended pressure and temperature conditions and stirred at a rate of 350 s^{-1}. To study rheological properties of foamed fluids the base fluid was first foamed with nitrogen. To this end approx. 500 ml of the tested fluid was placed in the fluid container (Figure 1). Then, by means of pumps, it was pumped into tubes of the measuring system. After its filling and venting the fluid circulation started in the measuring system, stabilising at the same time the temperature and pressure (6.89 MPa, T = 23 °C). Next, gas was additionally pumped to the measuring system, circulating the fluid continuously at a shear rate of 350 s^{-1}. At the same time the fluid was partially collected from the system, and then a partially foamed fluid, increasing thereby the gas share in the foam. The process was carried out till the moment of obtaining 50% or 70% of the foam quality, which was controlled by a densimeter. Once the foam quality stabilised, measurements of rheological properties were started in accordance with the prepared test plan. The stability test lasted 80 minutes, at a pressure of 1000 psi, maintaining a shear rate of 100 s^{-1}. To measure rheological properties during measurement loops (at minute 13, 25, and 38) the shear rates were assumed as follows: 40, 100, 200, 300, 200, 100, 40 s^{-1}. During a measurement loop the shear rate was kept at each of aforementioned levels for 60 seconds, to obtain a stable result. Between measurements the foam was stirred at a rate of 100 s^{-1} during 10 minutes. The foam half-time was determined after generating foam of 50% or 70% quality; the fluid flow through the rheometer was stopped and the foam was closed in the measurement chamber to maintain static measurement conditions. It is defined as the time, after which a half of water phase will be separated from the generated foam [50] and it is an important parameter describing the foam stability. Table 4 presents results of half-time measurements for S.F.

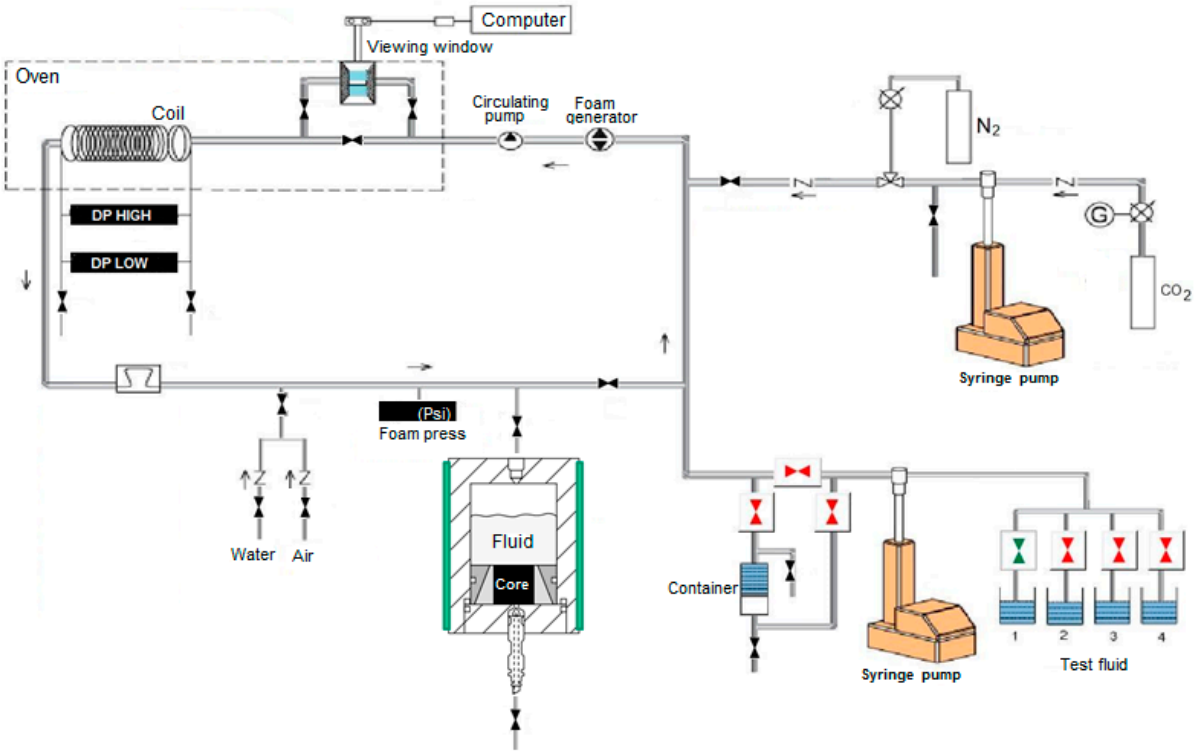

Figure 1. Measuring system to study the damage to the core by fracturing fluids with addition of N_2/CO_2 gases.

2.2. Induced Formation Damage

To a large extent the damaging tests consisted in pumping through the cores appropriate fracturing fluids, causing damage to the core material at the assumed pressure difference, like it is the case during actual reservoir stimulating treatments.

To simulate the formation damage by fracturing fluids, taking into account the impact of process fluids on the reservoir rock, a measuring system to test the cores' damage was used. To identify the reservoir formation damage it was necessary to appropriately prepare the cores. Samples to perform tests of rock damage by a fracturing fluid (non-foamed or with 50% content of N_2) were prepared from the core material. First, core plugs were cut out by a diamond crown, 3.81 cm in diameter and approx. 2.54 cm high; after cutting they were dried and placed in a desiccator. A decision was made to cut plugs of a larger diameter to have during the tests as high as possible pore volume and also as large as possible front surface of cores, on which the filtration cake will form. Core plugs prepared in such a way were subject to measurements of the permeability coefficient for gas and of the porosity ratio. The results of carried out measurements are specified in Table 5. Then the core plug was set in the measuring chamber using high-temperature silicone. Next the remaining components of the measuring chamber were screwed together and it was left for approx. 24 hours. After that period the chamber was thermostated up to 60 °C and the measurement started. The core was initially saturated with a 2% KCl solution at a constant rate by means of a constatimetric pump and then the chamber was filled with an appropriate fracturing fluid, and a pressure of 6.89 MPa (1000 psi) was applied. After opening a valve at the chamber bottom the core damaging started, lasting 50 minutes.

2.3. Rock Cores Samlpe Damage Examination

The use of a HRM-300 3D (Huvitz, South Korea) optical microscope with profiler and digital equipment and of Panasis software allowed to image the rock samples damage. For each core after damage 3 surface profiles were made using a reference plane - the surface without contact with the stimulation fluid (without filtration cake). The determined profile comprised the area from the core

centre to the wall of the rock mini-cylinder (5000 μm). The cake height was determined taking into consideration average roughness from roughness profiles along selected measurement sections.

An FEI Quanta 650 FEG (Thermo fisher scientific, USA) scanning electron microscope was used to make pictures and SEM analyses. The Quanta microscope is equipped with a field emission gun (FEG). The core photographs were made using a detector of backscattered electrons (BSE). Based on differences in the image scale of grey a phase contrast is visible on the samples surface (heavier minerals are lighter on the image, while lighter ones - darker). High and low vacuum was used for imaging. Low vacuum was used to avoid 'sample charging' (charge gathering in non-conducting places). The degree of damage was compared for cores, through which non-foamed fracturing fluid was pumped, with cores through which foamed fracturing fluid was pumped.

To observe the core plug damage not only on the front surface, but also outside, the core was split transversally into two parts, reproducing a natural rock fracture. It enabled more detailed observations of the range of the rock sample damage by fracturing fluids.

3. Results

3.1. Viscosity Measurements

Figs. 2-5 present results of rheological properties measurements for non-foamed and with nitrogen addition fracturing fluids. Measurements of rheological properties for all tested foamed and non-foamed fluids were carried out at 23 °C. The rheological parameters (n′ and K′) are presented in Tables 1-3, where n is the dimensionless flow index, and K is the consistency factor.

Table 1. Rheological parameters of fluids energised with N_2 with the application of Aerosil nanoadditive, foam quality of 50% and 70%.

S.F. composition		Q_f [%]	t [min]	n′ [-]	K′ [Pa·sⁿ′]	Dynamic viscosity at a given γ [mPa·s]		
						40s^{-1}	100s^{-1}	170s^{-1}
Water 0,4 % A, 0,1% Areosil	1a	No-foamed	13	0,9988	0,000022	2	2,3	2,5
			25	0,9989	0,000026	2,1	2,4	2,6
			38	0,9989	0,000027	2	2,3	2,4
	1b	50	13	0,5565	0,002466	23	15,3	12,1
			25	0,4125	0,00512	28,1	16,4	12
			38	0,5116	0,003098	24,5	15,6	12,1
		70	13	0,4479	0,007347	45,9	27,7	20,6
			25	0,5551	0,004069	37,7	25,1	19,8
			38	0,5939	0,003564	38,2	26,3	21,2

Table 2. Rheological parameters of fluids energised with N_2 with the application of U-2 nanoadditive, foam quality of 50% and 70%.

S.F. composition		Q_f [%]	t [min]	n′ [-]	K′ [Pa·sⁿ′]	Dynamic viscosity at a given γ [mPa·s]		
						40s^{-1}	100s^{-1}	170s^{-1}
Water 0,4 % A, 0,1% U-2	2a	No-foamed	13	0,9907	0.0026	2,6	2,5	2,5
			25	0,999	0.0021	2,4	2,5	2,6
			38	0,999	0.0024	2,6	2,6	2,6
	2b	50	13	0,4816	0,003417	24,2	15	11,4
			25	0,5403	0,002568	22,6	14,8	11,6
			38	0,642	0,001544	19,7	14,2	11,8

Preprints (www.preprints.org) | NOT PEER-REVIEWED | Posted: 28 April 2019 doi:10.20944/preprints201904.0313.v1

Peer-reviewed version available at Nanomaterials 2019, 9, 766; doi:10.3390/nano9050766

		70	13	0,5923	0,007221	76,8	52,9	42,6
			25	0,6662	0,005006	69,9	51,5	43,1
			38	0,4845	0,011807	84,4	52,6	40

Table 3. Rheological parameters of fluids energised with N_2 with the application of U-2 nanoadditive and natural polymer, foam quality of 50% and 70%.

S.F. composition		Q_f [%]	t [min]	n′ [-]	K′ [Pa·s$^{n'}$]	Dynamic viscosity at a given γ [mPa·s]		
						40s^{-1}	100s^{-1}	170s^{-1}
Water 0,4 % A, 0,1% U-2 0,1% W	3a	No-foamed	13	0,9989	0.0019	2,9	3,3	3,5
			25	0,9989	0.0017	2,5	2,8	3
			38	0,9989	0.0014	2,5	2,8	3,1
	3b	50	13	0,4283	0,006129	35,6	21,1	15,6
			25	0,4123	0,006996	38,3	22,4	16,4
			38	0,4187	0,006726	37,7	22,1	16,3
		70	13	0,7154	0,004226	70,8	54,6	46,9
			25	0,7277	0,004209	73,8	57,5	49,8
			38	0,7496	0,004297	81,7	64,9	56,9

Table 4. Measurements of foamed S.F. half-time with addition of 50% and 70% of N_2.

S.F. composition	Q_f [%]	Foam half-time [s]
4 ml/l A	50	30
4 ml/l A	70	60
0,1% Areosil, 4 ml/l A	50	60
0,1% Areosil, 4 ml/l A	70	90
0,1% U-2, 4 ml/l A	50	80
0,1% U-2, 4 ml/l A	70	240
0,1% U-2, 4 ml/l A, 0,1% W	50	360
0,1% U-2, 4 ml/l A, 0,1% W	70	390

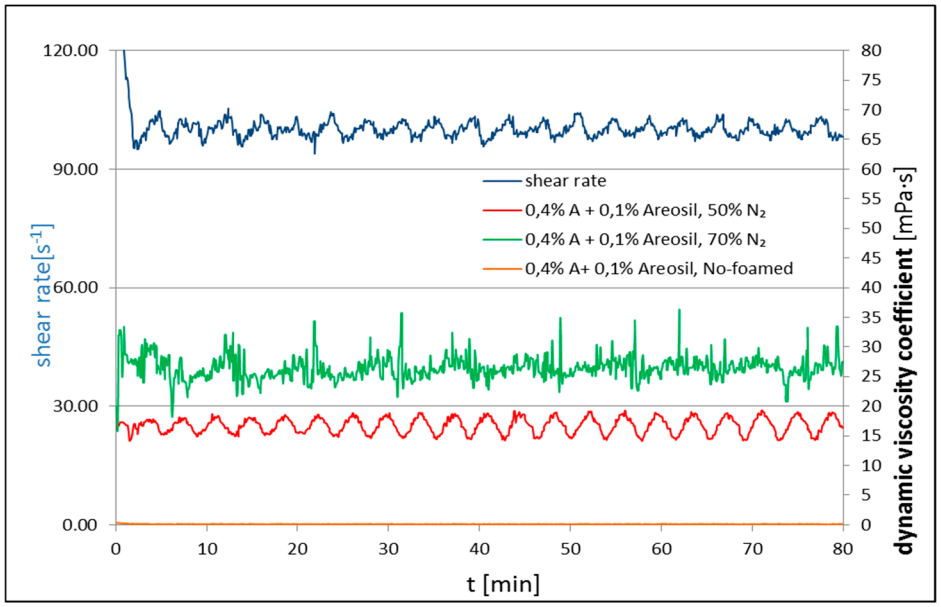

Preprints (www.preprints.org) | NOT PEER-REVIEWED | Posted: 28 April 2019 doi:10.20944/preprints201904.0313.v1

Peer-reviewed version available at Nanomaterials 2019, 9, 766; doi:10.3390/nano9050766

Figure 2. Viscosity of non-foamed and N_2 foamed fluid of 50% and 70% quality at 23 °C at a shear rate of 100s^{-1}.

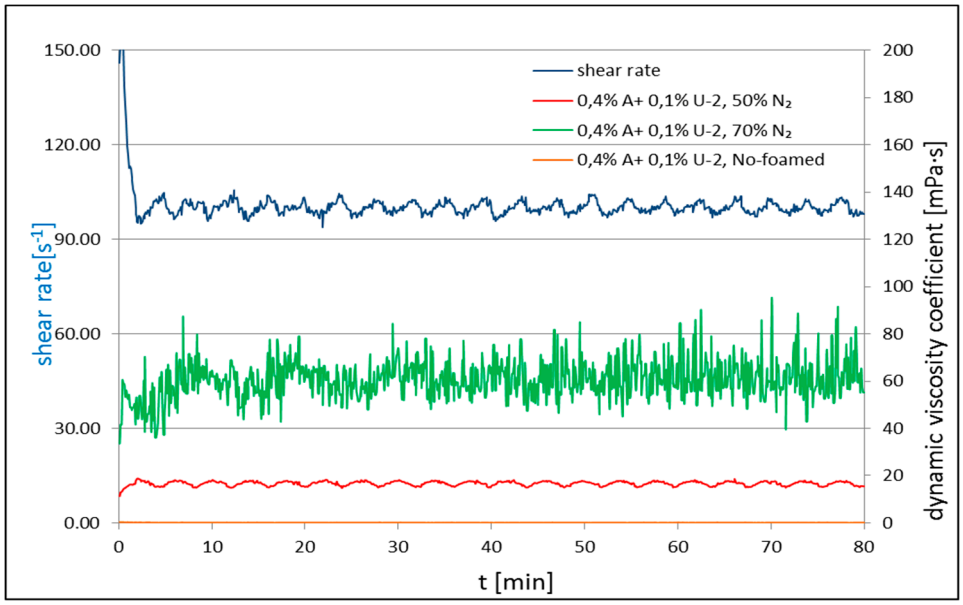

Figure 3. Viscosity of non-foamed and N_2 foamed fluid of 50% and 70% quality at 23 °C at a shear rate of 100s^{-1}.

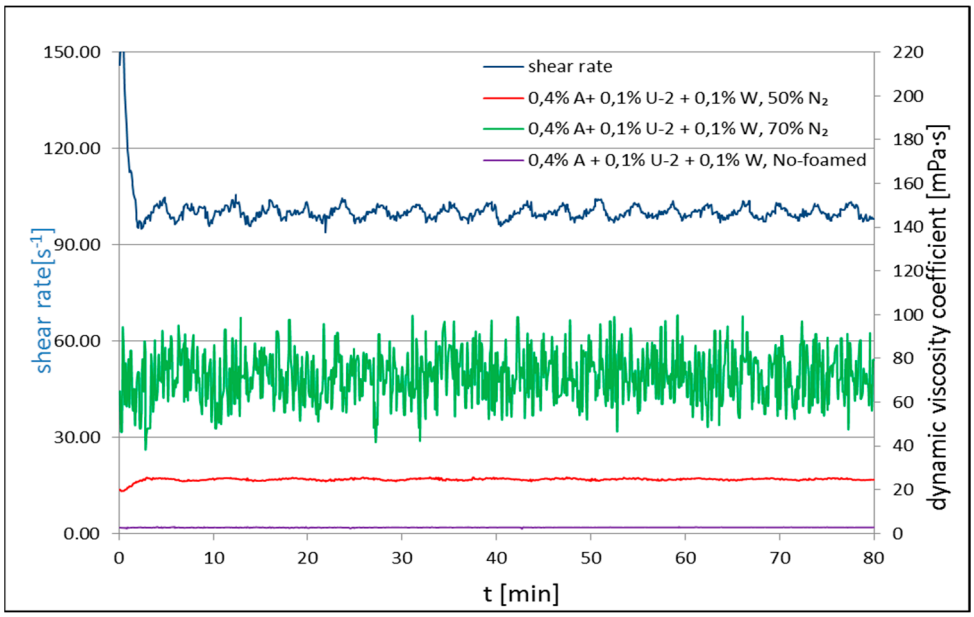

Figure 4. Viscosity of non-foamed and N_2 foamed fluid of 50% and 70% quality at 23 °C at a shear rate of 100s^{-1}.

Graphs 2-4 present the apparent viscosity registered during the test for process fluid solutions with addition of a surfactant, nanoadditives Aerosil 300 (Figure 2) or U-2 (Figure 3), and polymer in certain cases (Figure 4). For each composition of additives two tests were performed: to measure n' and K' (Tables 1–3) and the measurement of apparent viscosity over time (Figures 2–4). Each time basic rheological parameters were tested for the foam of 50% and 70% quality. Nanoadditive Aerosil 300 was used in the first series of tests. The initial viscosity of 50% foam with the addition of only a foamer and the nanoadditive was 16 cP and 26 cP (Q_f = 70%) at 100 s^{-1}. The non-foamed fluid featured the viscosity of approx. 2 cP at 100 $^{-1}$. In the second series of tests the U-2 nanoadditive was used at the amount of 0.1% vol. The viscosity with the addition of only a surfactant and the

nanoadditive was 15 cP in the case of foam at a temperature of 23 °C and 50% quality, and 52 cP for the foam of 70% quality. After adding 0.1 wt. % of natural polymer to U-2 nanoparticles the viscosity went up to 22 and 55 cP for the tested foam qualities, respectively. The nanoparticles addition increases stability of the foamed fluid, which was confirmed by authors of paper [51]. The increased stability may be confirmed also when analysing the half-time. It increases 12 times in the case of 50% nitrogen content in the fluid with U-2 addition and polymer, and 6.5 times for the 70% foam as compared with the fluid without the SiO_2 addition.

3.2. Formation Damage Evaluation

Table 5. Results of porosity ratio and permeability coefficient measurement before and after performance of damaging tests.

Fluids injected through the core		core number	k_0 [md]	k_k [md]	% k_{red}	ϕ_0 [%]	ϕ_k [%]	% ϕ_{red}
S.F. 1a	0,1 % Areosil, 4ml/l A No-foamed	3231	5,03	1,93	61,00	15,05	13,53	10,09
S.F. 1b	0,1 % Areosil, 4ml/l A Foamed with N_2	3232	4,72	2,78	41,10	15,20	13,84	8,95
S.F. 2a	0,1 % U-2 4ml/l A No-foamed	3226	4,11	2,06	49,88	15,70	13,37	14,81
S.F. 2b	0,1 % U-2 4ml/l A Foamed with N_2	3224	3,96	2,99	24,49	15,07	14,60	3,12
S.F. 3a	0,1 % U-2 4ml/l A 0,1 % W No-foamed	3233	7,65	2,32	69,67	15,80	14,08	8,10
S.F. 3b	0,1 % U-2 4ml/l A 0,1 % W Foamed with N_2	3229	6,92	4,82	30,35	15,77	15,38	2,47

The permeability coefficient was significantly decreasing, in particular in the case of cores treated with non-foamed process fluids. Foamed fluids caused a smaller permeability and porosity reduction than non-foamed fluids. The biggest damage to permeability was caused by non-foamed fluids with the addition of polymer W (fig. 5). The estimated permeability damage was approx. 20% smaller for foamed fluids as compared with fluids without the nitrogen addition. Concentration of nanoparticle suspension, well-dispersion solution, injection rate, and pore volume injected are the most important parameters affecting the permeability impairment [52].

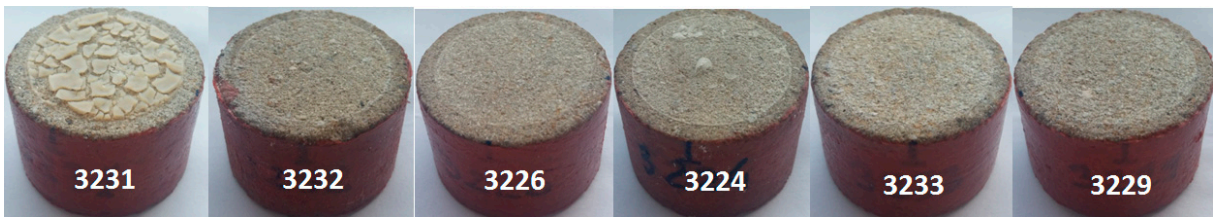

Figure 5. The cores surface after damage with S.F.

Peer-reviewed version available at Nanomaterials 2019, 9, 766; doi:10.3390/nano9050766

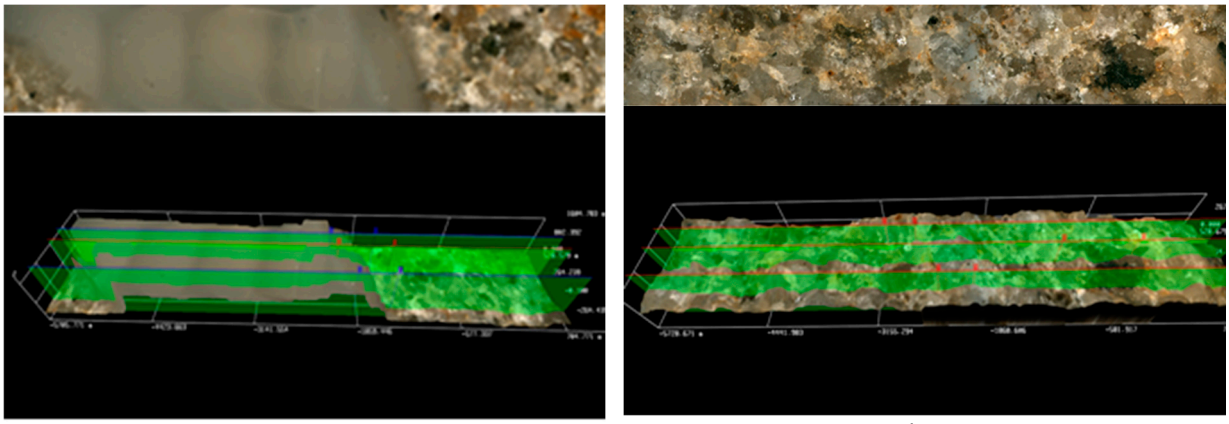

(a) (b)

Figure 6. Results of microscopic analysis of the front surface of core No 3231 and 3232 after the damaging test S.F.: a) 1a, b) 1b.

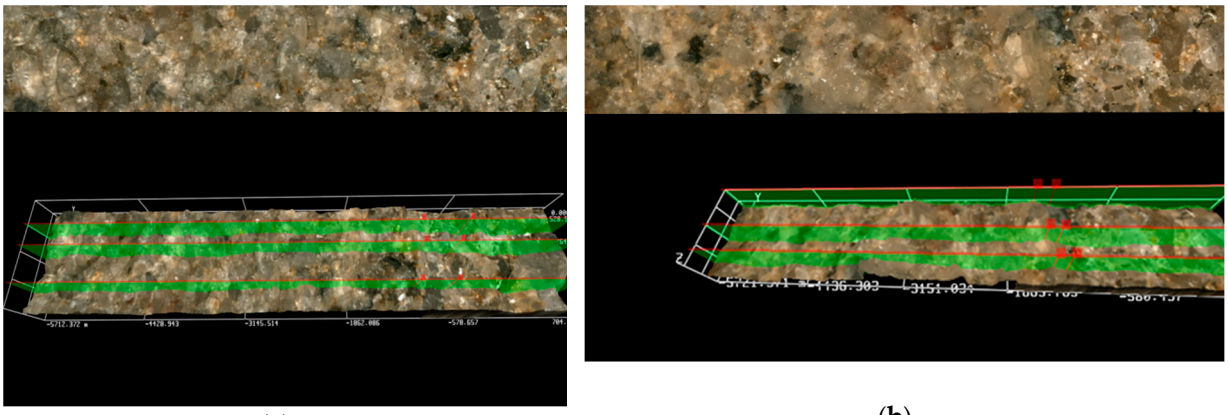

(a) (b)

Figure 7. Results of microscopic analysis of the front surface of core No 3226 and 3224 after the damaging test S.F.: a) 2a, b) 2b.

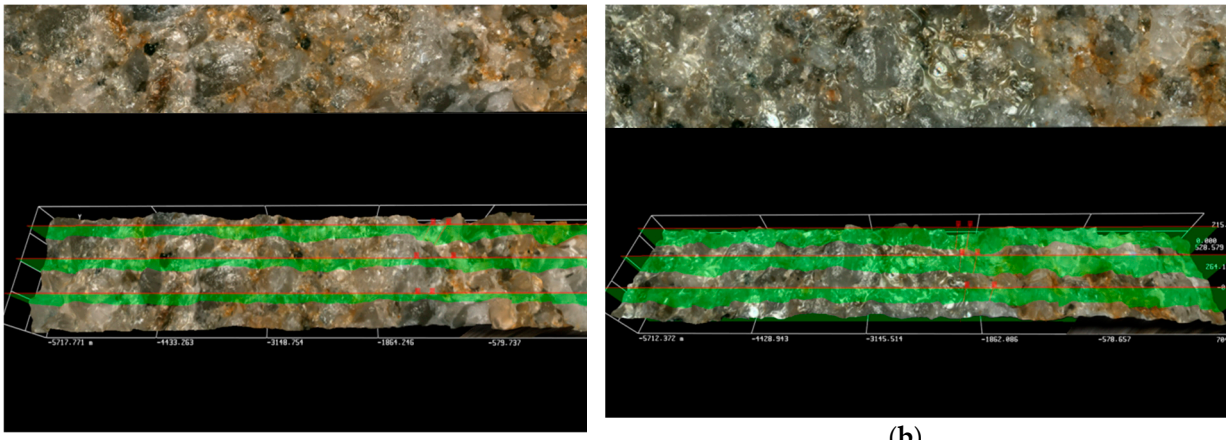

(a) (b)

Figure 8. Results of microscopic analysis of the front surface of core No 3233 and 3229after the damaging test S.F.: a) 3a, b) 3b.

The filtration cake height was determined thanks to the 3D software in the optical microscope, using an arithmetical mean of three selected areas on the front surface of the tested rock sample. An average height of the cake for non-foamed fluids ranged between 1161 and approx. 108 μm. Instead, in the case of cores treated with foamed fracturing fluids, the measured filtration cake was definitely thinner and was from a few dozen to approx. a dozen μm thick. Figure 6 presents the front surface of

Peer-reviewed version available at Nanomaterials 2019, 9, 766; doi:10.3390/nano9050766

cores 3231 and 3232 after pumping through it the fluid with Aerosil addition, non-foamed (Figure 11a) and foamed (Figure 11b), respectively. A layer of filtration cake is especially visible on the profile of non-foamed fluid (Figure 11a). Results of presented tests show that the N_2 foamed fluid based on nanoparticles with the addition of a foamer and U-2 additive is least invasive (Figure 7b). Only small traces of a filtration cake in the form of an uneven coating are visible on the surface. In the case of filtration of fluid based on polymer with nanoparticles addition the filtration cake is best visible (Figure 8a and 8b). Its thickness in the case of U-2 application in a non-foamed fluid is estimated at approx. 170 μm (Figure 8a), while in the case of foamed fluids at approx. 110 μm (Figure 8b).

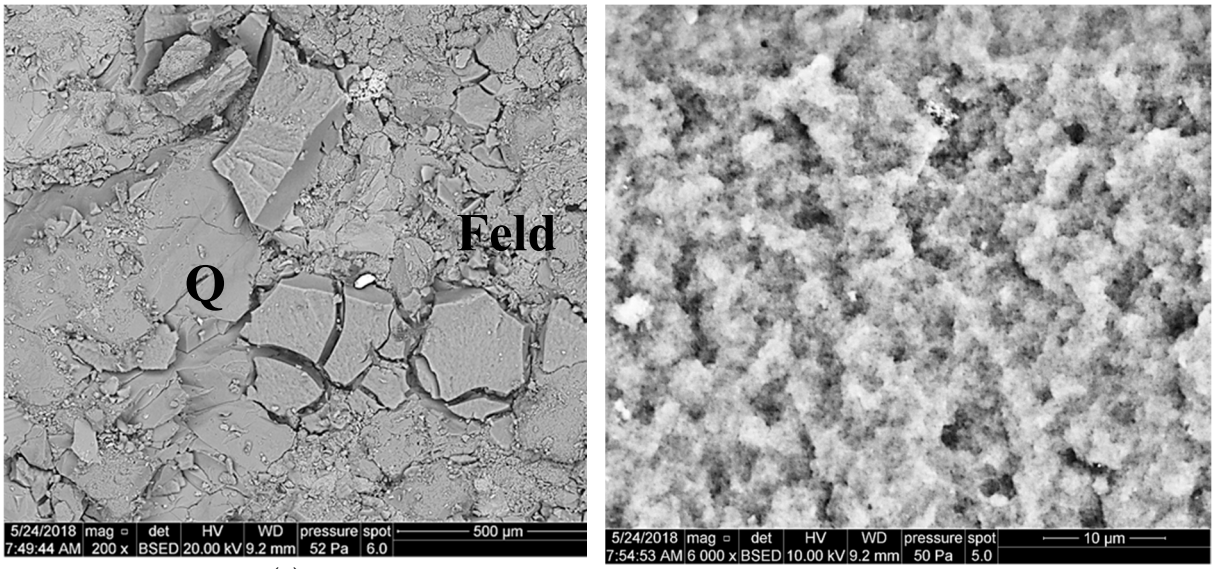

(**a**) (**b**)

Figure 9. SEM image of the 3231 core face after contact with Areosil S.F. 1a, a) top view of the core face; Q - quartz, Feld - feldspar, b) top view of the core face at a high magnification.

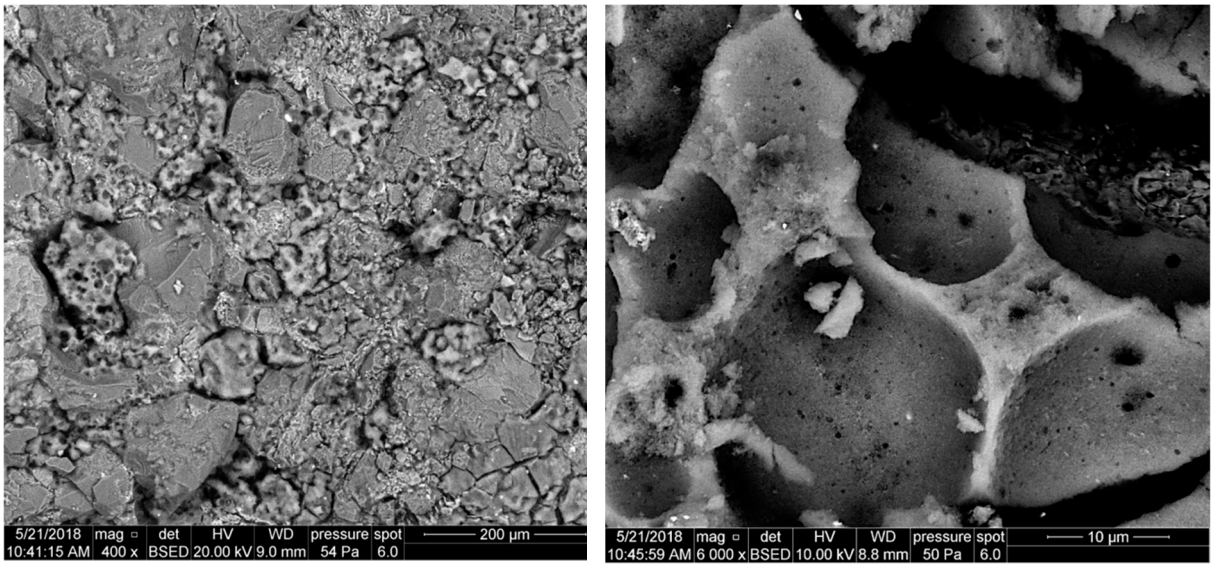

(**a**) (**b**)

Figure 10. SEM image of the 3232 core face after contact with foamed Areosil S.F. 1b, a) top view of the core face, b) top view of the core face at a high magnification.

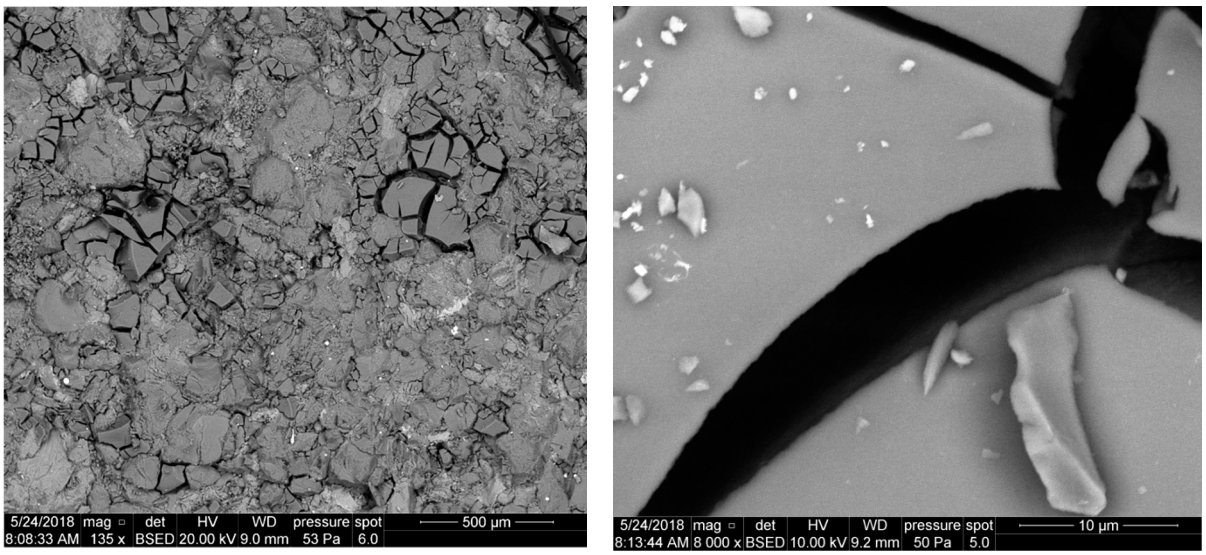

(**a**) (**b**)

Figure 11. SEM image of the 3226 core face after contact with U-2, S.F. 2a, a) top view of the core face, b) top view of the core face at a high magnification.

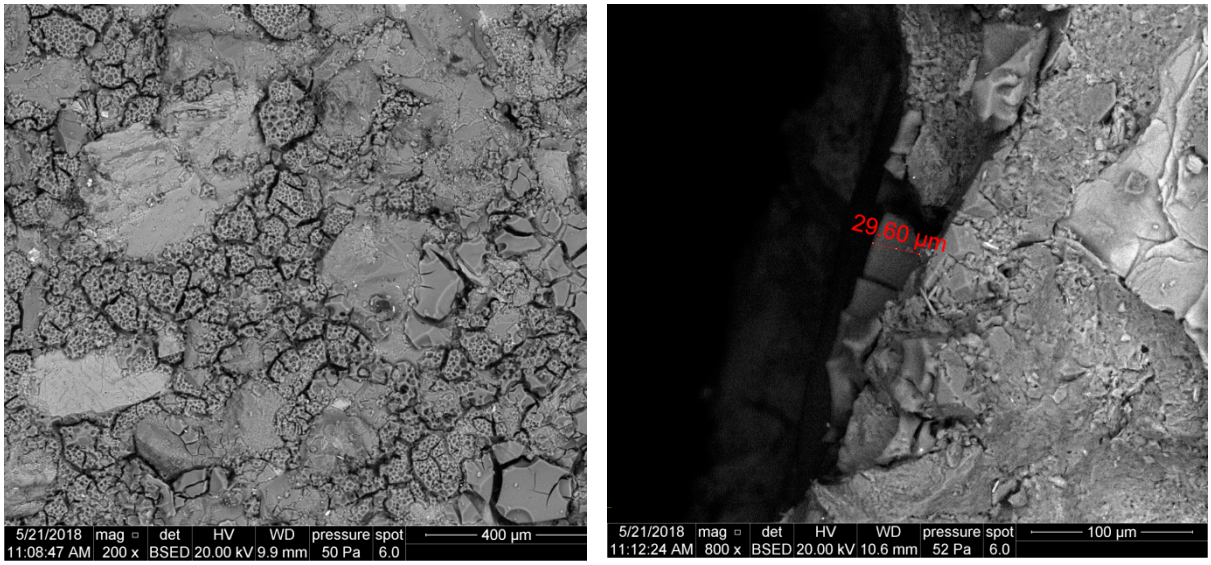

(**a**) (**b**)

Figure 12. SEM image of the 3224 core face after contact with foamed U-2 S.F. 2b, a) top view of the core face, b) side view of the core face.

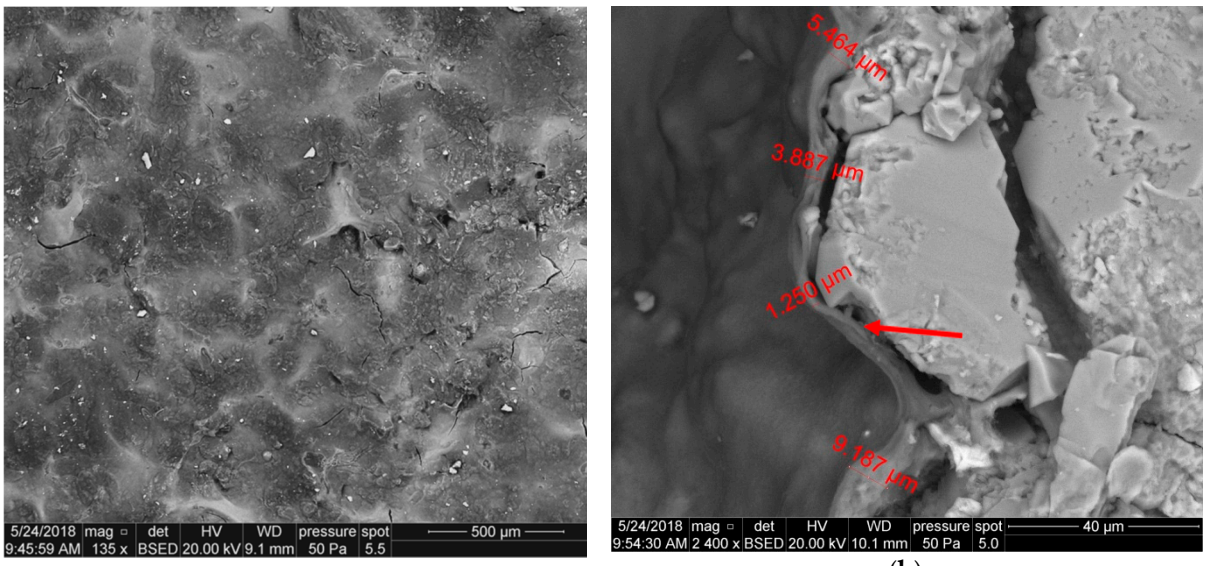

(**a**) (**b**)

Figure 13. SEM image of the 3233 core face after contact with U-2 S.F. 3a, a) top view of the core face, b) side view of the core face.

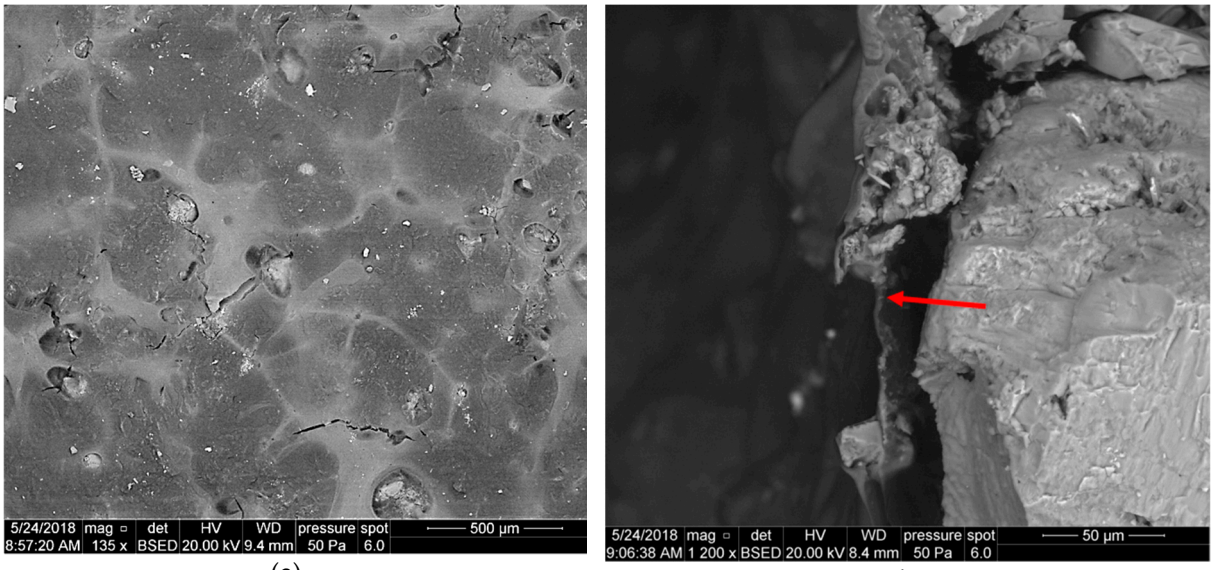

(**a**) (**b**)

Figure 14. SEM image of the 3229 core face after contact with foamed U-2 and polimer S.F. 3b, a) top view of the core face, b) side view of the core face.

Figure 9 presents the front surface of core 3231 after the core damage with the fluid with Aerosil additive - 1a. The filtration cake coating (Figure 9a) is a silica gel; it exists only in fragments, is strongly crushed and fills cavities between detrital rock components (quartz and feldspars). It is possible to distinguish one type of cake fragments: fragments with a flat but slightly lumpy surface. Figure 9b is a filtration cake coating (silica gel) at a high magnification. The surface is uneven, and relief elements are spread irregularly. The cake structure is not uniform, it seems to be formed of grains much smaller than 1 µm.

In the case of foamed fluid application - 1b, the front surface of the sample is covered with a highly crushed coating, filling cavities between the quartz grains (Figure 10a). In the close-up one can see fragments of the cake with a porous surface, with finer cavities after gas bubbles up to a dozen or so micrometres in diameter (Figure 10a). The structure reveals sub-micron elements forming the coating.

Figure 11 presents the surface of sample 3226. The cake coating is strongly crushed and fills cavities between detrital rock components (Figure 11a). It is possible to distinguish polymer fragments with a smooth surface; cavities after gas bubbles are not visible. Fractures are visible on the magnification of a cake fragment; small white crystals are KCl, which crystallised from the pad fluid (Figure 11b).

Figure 12a shows a polymer coating, which is strongly crushed and fills cavities between detrital rock components (quartz and feldspar) of sample 3224. It is possible to distinguish two types of polymer fragments: 1) - fragments with a smooth surface, with possibly noticeable cavities after gas bubbles, a few dozen μm in diameter, 2) - fragments with a porous surface, covered with finer cavities after gas bubbles, up to a dozen or so μm in diameter. The presence of those two types suggests zonal differentiation of fluid viscosity and surface tension. Photograph 12b presents the front surface of sample - a side view. The cake coating, approx. 30 μm thick, is visible only on the surface.

The filtration cake coating on core 3233 it is characterized by considerable continuity, which is related to the addition of polymer W, but with finely diversified relief: shallow pseudo-polygonal cavities and few irregular fractures are marked. Occasionally existing small mineral fragments are dispersed on the polymer surface - Figure 13a. Figure 13b presents the front surface of sample 3233 - a side view. A uniform polymer coating (red arrow) is a few μm thick.

In the case of foamed fluid 3b the coating on the core surface (Fig. 14a) is also continuous, with finely diversified relief and shallow pseudo-polygonal cavities. Contrary to sample 3223 (Figure 13a) oval cavities are visible, probably related to gas bubbles, with dimensions up to 150 μm. These cavities reveal the rock grains, that are lying under the coating. Small mineral fragments are dispersed sparsely on the polymer layer surface.

Figure 14b presents the front surface of sample - a side view. Uniform polymer coating, a few μm thick, is contaminated with mineral particles. The coating separates from the rock surface, which can result from polymer drying and sample splitting.

4. Discussion

1. The knowledge of rheological parameters of base fluids is indispensable to prepare a design of technological treatment. On this basis fracturing fluids are selected for a specific type of reservoir rock and for the reservoir conditions. They also prove a specific fluid's potential to transport the proppant. Apparent viscosity was studied for process fluid solutions with addition of surfactant A, nanoadditives U-2 or Aerosil 300, and in certain cases of polymer W. Each time basic rheological parameters were studied for the foam of 50% and 70% foam quality at 23 °C. Viscosity of 50% foam with addition of a foamer and of both nanoadditives did not differ and was approx. 15 cP. The viscosity coefficient of foam (at Qf = 70%) with U-2 addition was much higher than that with Aerosil additive. After polymer addition to U-2 nanoparticles the viscosity significantly increased, in particular at 50% foam quality. The viscosity grows from a few cP for the non-foamed fluid to a few dozen cP in the case of foam with the nanoadditive and natural polymer; the foaming resulted in a dozen or so times increase in S.F. viscosity and in its stability, which was confirmed also by the half-time measurement.

2. The permeability coefficient was significantly decreasing, in particular in the case of cores treated with non-foamed process fluids. Foamed fluids caused a smaller permeability and porosity reduction than non-foamed fluids. The biggest damage to permeability was caused by a non-foamed fluid with the addition of polymer W. The addition of nanoparticles caused also reduction of permeability, in particular after the application of Aerosil. Instead, the addition of U-2 sol did not result in a significant reduction of the permeability coefficient, especially after the fluid foaming with N_2. The estimated permeability damage was approx. 20% smaller for foamed fluids as compared with fluids without the nitrogen addition.

3. An average height of the cake for non-foamed fluids, determined thanks to 3D software in the optical microscope, ranged between 1161 and approx. 30 μm. Instead, in the case of cores treated with foamed fracturing fluids, the measured filtration cake was definitely thinner and was from a few dozen to approx. a dozen μm thick. The results of presented studies show that the foamed fluid based on U-2 nanoparticles with a foamer addition is least invasive. Only small traces of a filtration cake in the form of an uneven coat are visible on the surface. Its thickness in the case of U-2 application is estimated at approx. 63 μm, while in the case of fluid with Aerosil 300 addition at approx. 1161 μm.

4. The SEM analysis allowed to determine the filtration cake thickness, and also the polymer presence in the analysed rock material. The results of presented SEM studies show that least invasive are foamed fluids, forming an irregular flaky coating of core surfaces, which is consistent with the analysis by means of an optical microscope and a profilometer. Nanoadditives affected the formation of filtration cake on the sample's surface, especially during cores damaging with a non-foamed fluid with the Aerosil additive. During the non-foamed fluids filtration the filtration cake was creating a pretty compact and more even coating. Its thickness ranges from a few to a few dozen μm.

5. Taking into consideration the foam stability, rheology parameters, and the degree of damage, a foamed fracturing fluid based on 0.1 % of U-2 with addition of 4 ml/l of surfactant is the best fluid. The experimental data showed that the stability foam increased when silica (SiO_2) nanoparticles were added. SiO_2 nanoparticle-surfactant-stabilized foam for fracturing is superior to traditional water based fracturing fluids and causes lower core permeability damage than a traditional F.F. It is recommended for use in hydraulic fracturing, particularly for fracturing stimulation in tight and shale gas reservoirs. The obtained results demonstrate that the suitability of adding nanoparticles to fracturing fluid for stimulations will improve its performance.

Author Contributions: Conceptualization, K.W., P.K. and K.L.; Formal analysis, K.W.; Investigation, K.W., P.K., K.L. Methodology, K.W. and P.K.; Resources, K.W.; Supervision, P.K. and K.L.; Validation, K.W, P.K. and K.L.; Writing—original draft, K.W.; Writing—review&editing, P.K., K.L and KW.

Funding: Part of the research leading to these results was prepared on the basis of statutory study financed by Ministry of Science and Higher Education – archival no.: 0010/KS/18, order no.: DK-4100-10/18.

Acknowledgments: The authors would like to thank the Oil and Gas Institute – National Research Institute, Poland, for providing access to laboratory equipment. Authors thank Evonik Industries for supplying Aerosil 300 and Witchem company for supplying U-2 nanofluid, CESI for Foamer A and Weatherford for polymer used in this study.

Conflicts of Interest: The authors declare no conflict of interest.

Abbreviations

The following abbreviations are used in this manuscript:

$\%k_{red}$ permeability reduction
$\%\phi_{red}$ porosity reduction
A anionic foamer
EOR Enhanced oil recovery
F Feld feldspar
F.F. Fracturing fluids
HF hydraulic fracturing
HPG hydroxypropyl guar
K consistency factor
k_0 initial core permeability
k_k final core permeability

n flow index
Q quartz
Q_f foam quality
S.F. stimulation fluids
T temperature
t test time
TEOS tetraethoxysilane
W fast hydrating guar gum (HPG)
γ shear rate
ϕ_0 initial core porosity
ϕ_k final core porosity

References

1. Bentley, R. W. Global oil & gas depletion: an overview. *Energy Policy* **2002**, 30, 189–205. doi.org/10.1016/S0301-4215(01)00144-6.
2. Lubaś, J., Szott, W., Dziadkiewicz, M. Analiza możliwości zwiększenia stopnia sczerpania zasobów złóż ropy naftowej w Polsce. *Nafta-Gaz* **2012**, 8, 481-489.
3. Bhattacharyya, S.C. Energy Economics: Concepts, Issues, Markets and Governance, 1nd ed.; Springer-Verlag London; **2011**, 1-5. ISBN 978-0-85729-268-1.
4. Bohloli, B., de Pater, C.J. Experimental study on hydraulic fracturing of soft rocks: Influence of fluid rheology and confining stress, Journal of Petroleum Science and Engineering, **2006**, Vol. 53, Issues 1–2, 1-12. DOI.https://doi.org/10.1016/j.petrol.2006.01.009.
5. Guo, B.; Liu, X.; Tan, X. Hydraulic Fracturing, In Petroleum Production Engineering, 2nd ed.; Gulf Professional Publishing, Elsevier, **2017**, ISBN 9780128096123.
6. McAleese, S. Test Design, In Operational Aspects of Oil and Gas Well Testing, Elsevier, **2000**; 1, pp. 57-70, ISBN: 978-0-444-50311-4.
7. Gharibi, A.; Zoveidavianpoor, M.; Ghadikolaei, F.D. On the Application of Well Stimulation Method in Improvement of Oil Recovery. Applied Mechanics and Materials, **2015**, 735, 31-35. doi.org/10.4028/www.scientific.net/AMM.735.31.
8. Tunio, S.Q., Tunio, A.H., Ghirano, N.A., El Adawy, Z.M. Comparison of Different Enhanced Oil Recovery Techniques for Better Oil Productivity. Int. J. of Appl. Sci. and Technol., **2011**, 1, 143-153.
9. Karadkar, P., Bataweel, M., Bulekbay, A., Alshaikh A.A.: Energized Fluids for Upstream Production Enhancement: A Review. SPE-192255-MS. Society of Petroleum Engineers, **2018**, 1-26. doi.org/10.2118/192255-MS.
10. Hou, Q., Zhu, Y., Luo, Y., Weng, R. Studies on Foam Flooding EOR Technique for Daqing Reservoirs After Polymer Flooding. SPE-151955-MS, **2012**. DOI 10.2118/151955-MS.
11. Dankwa, O., Appah, D., Joel, O.F., Asiam, E.K. Compatibility: A Key To An Efficient Matrix Acidizing Fluid Design. *J Pet Environ Biotechnol* **2016**, 7, 1-5. doi:10.4172/2157-7463.1000274.
12. Subhash, N.S., Patel, H., Pandy, S. Motion of Fracturing Fluid and Associated Environmental Impacts Conference Paper: Conference: NSF sponsored workshop: Reducing the Impact of Hydraulic Shale Fracturing and Natural Gas Drilling on Environments: Development of Green Fracturing Fluids and Sustainable Remediation and Containment Technologies, At The University of Arkansas at Little Rock, Arkansas, **2015**, 1-22.
13. Taber, J.J., Martin, F.D., Sergiht, R.S. EOR screening criteria revised – Part 1, : Introduction to Screening Criteria and Enhanced Recovery Field Projects. SPE-35385-PA, Society of Petroleum Engineers, **1997**, 12(3):189-198. doi.org/10.2118/35385-PA.
14. Yuan, B., Wood, D.A. A comprehensive review of formation damage during enhanced oil recovery. *J. Petr. Sci. Eng.* **2018**, 167, 287-299. doi.org/10.1016/j.petrol.2018.04.018.
15. Sheng, J.J. Formation damage in chemical enhanced oil recovery processes. *Asia-Pacific. J. Chem. Eng.* **2016**; 11, 826-835. doi.org/10.1002/apj.2035.

16. Reinicke, A., Rybacki, E., Stanchits, S., Huenges, E., Dresen G. Hydraulic fracturing stimulation techniques and formation damage mechanisms—Implications from laboratory testing of tight sandstone–proppant systems. *Geochemistry* **2010**, 70, 107-117. doi.org/10.1016/j.chemer.2010.05.016.
17. Yekeenac, N.,. Manan, M.A., Idrisb, A.K., Padmanabhanc, E., Junina, R., Samina, A.M., Gbadamosia, A.O., Oguamahd, I. A comprehensive review of experimental studies of nanoparticles-stabilized foam for enhanced oil recovery. *J. Petr. Sci. Eng.* **2018**, 164, 43-74. doi.org/10.1016/j.petrol.2018.01.035.
18. Qajar, A., Xue. Z., Worthen., A.J., Johnston. P.K., Huh. C., Bryant S.L., Prodanović, M. Modeling Fracture Propagation and Cleanup for Dry Nanoparticle-Stabilized-Foam Fracturing Fluids, *Journal of Petroleum Science and Engineering*, **2016**, 146, 210-221. DOI: 10.1016/j.petrol.2016.04.008
19. Yekeen, N., Manan, M.A., Idris, A.K., Gbadamosi, A.O. A comprehensive review of experimental studies of nanoparticles-stabilized foam for enhanced oil recovery, *Journal of Petroleum Science and Engineering*, **2018,** 164, 43-74. DOI: 10.1016/j.petrol.2018.01.035.
20. Zhang, T., Roberts, M., Bryant, S.L., Huh, C. Foams and Emulsions Stabilized With Nanoparticles for Potential Conformance Control Applications, *SPE-121744-MS*, **2009**, 1-17. DOI. https://doi.org/10.2118/121744-MS.
21. Singh, R., Mohanty, K.K. Nanoparticle-stabilized foams for high-temperature, high-salinity oil reservoirs, SPE-187165–MS, **2017**, 1-15. Proceedings of the SPE Annual Technical Conference and Exhibition, San Antonio, Texas, USA. https://doi.org/10.2118/187165-MS.
22. Gidley L.J., S.A. Holditch, D.E. Nierode, W.R. Veatch, SPE Monograph Series **1989**, 12, 198.
23. Chaudhary, S., Singh, S., Singh, V.K. A Novel approach for formulating CO2 Foam Based Fracturing Fluid by Synthesized Grafting Copolymerization to Enhance its Stability for HPHT Shale Reservoirs, *Petro. Chem. Indus. Intern.*, **2019**, vol.2, issue 2, 1-6, ISSN: 2639-7536.
24. Wanniarachchi, W. A. M., Ranjith, P. G., Perera M. S. A., Lashin, A., . Al Arif, N., Li, J. C. Current opinions on foam-based hydro-fracturing in deep geological reservoirs, *Geomechanics and Geophysics for Geo-Energy and Geo-Resources*, **2015**, Vol. 1, Issue 3–4, 121–134. DOI https://doi.org/10.1007/s40948-015-0015-x.
25. Kong, X., McAndrew, J., Cisternas, P. CFD Study of Using Foam Fracturing Fluid for Proppant Transport in Hydraulic Fractures, *SPE-183549-MS*, **2016**, 1-15. DOI. 10.2118/183549-MS.
26. Tong, S., Singh, R., Mohanty, K.K. A visualization study of proppant transport in foam fracturing fluids. J Natural Gas Sci Eng **2018**, 52, 235-247. doi.org/10.1016/j.jngse.2018.01.030.
27. Laura, A. Analysis of fracturing fluid system, effect of rock mechanical properties on fluid selection. *AGH Drill Oil Gas* **2014**, 31(1), 167–178.
28. Wilk K., Kasza P., Czupski M.: Dobór dodatków do energetyzowanych płynów szczelinujących. *Nafta-Gaz* **2016**, 12, 1092-1100, DOI: 10.18668/NG.2016.12.12.
29. Yekeen, N., Padmanabhan, E., Idris, A.K. A review of recent advances in foam-based fracturing fluid application in unconventional reservoirs, *Journal of Industrial and Engineering Chemistry*, **2018**, Vol.66, 45-71, DOI.10.1016/j.jiec.2018.05.039.
30. Harris, P.C. Application of Foam to Minimize Damage During Fracturing. SPE 22394, **1992**, 1-6.
31. Kong, B., Wang, S., Chen, S., Don,g K. Minimize Formation Damage in Water-Sensitive Unconventional Reservoirs by Using Energized Fracturing Fluid. *SPE International Conference and Exhibition on Formation Damage Control*, 24-26 February **2016**, Lafayette, Louisiana, USA. SPE-179019-MS. doi.org/10.2118/179019-MS.
32. Bennion, D.B., Thomas, F.B., Bennion, D.W., Bietz, R.F. Mechanisms of Formation Damage and Permeability Impairment Associated With the Drilling. Completion and Production of Low API Gravity Oil Reservoirs. SPE 30320, *Society of Petroleum Engineers*, **1995**, 1-19. doi.org/10.2118/30320-MS.
33. Puthalath, R., Murthy, C.S.N., Surendranathan, A.O. Reservoir formation damage during various phases of oil and gas recovery - an overview. *International Journal of Earth Sciences and Engineering*, **2012**, 5(2), 224-231.
34. Fletcher, A.J.P., Daviss, J.P. How EOR Can be Transformed by Nanotechnology, SPE 129531-MS, **2010**, DOI: 10.2118/129531-MS.
35. Lau, H.C., Yu, M., Nguyen, Q.P. Nanotechnology for Oilfield Applications: Challenges and Impact. SPE-183301-MS **2016**, DOI https://doi.org/10.2118/183301-MS.
36. Gottardo, S., Mech, A.,Gavriel, M.,Gaillard, C.,Sokull-Klüttgen, B. Use of nanomaterials in fluids, proppants, and downhole tools for hydraulic fracturing of unconventional hydrocarbon reservoirs. *JRC Technical raport*, Publications Office of the European Union, **2016.**

37. Friedheim, J., Young, S., De Stefano, G., Lee, J., Guo, Q. Nanotechnology for Oilfield Applications – Hype or Reality? SPE 157032, **2012**, s. 1–7, DOI: 10.2118/157032-MS.
38. Montgomery, C. Fracturing Fluids, Intech **2013**
39. Ariza, C.A.F., Correa, F.B.C. Formation Damage in Oil and Gas Reservoirs: Nanotechnology Applications for its Inhibition/Remediation, Publisher: Nova Science Publishers, ISBN: 9781536139020, Inc (US) (2 Sept. **2018**).
40. Youssifa, M.I., El-Maghrabyb, R.M., Saleh, S.M., Elgibaly, A. Silica nanofluid flooding for enhanced oil recovery in sandstone rocks. *Egyptian Journal of Petroleum*,Volume 27, Issue 1, March **2018**, 105-110.
41. Habibi, A., Ahmadi, M., Pourafshary, P., Ayatollahi, S., Al-Wahaibi, Y. Reduction of Fine Migration by Nanofluids Injection, An Experimental Study, SPE-144196-PA, **2012**, 1-10. DOI:https://doi.org/10.2118/144196-PA.
42. Kong, X. Aplications of Mico and Nano Technologies in the Oil and Gas Industry – An Overview of the Recent Progress, SPE 138241-MS, **2010**, DOI: 10.2118/138241-MS.
43. Hendraningrat, L., Li, S., Torsæte, O. A Coreflood Investigation of Nanofluid Enhanced Oil Recovery in Low-Medium Permeability Berea Sandstone. SPE-164106, **2013**, s.1-14, DOI: 10.2118/164106-MS.
44. Aly, A.M. Understanding the Mechanism of Nanoparticles Applications in Enhanced Oil Recovery. SPE-175806-MS, **2015**; DOI: 10.2118/175806-MS.
45. McElfresh, P., Holcomb, D., Ector, D. Application of Nanofluid Technology to Improve Recovery in Oil and Gas Wells. **2012**, SPE 154827, DOI:10.2118/154827-MS.
46. Chengara, A., Nikolov, A. D., Wasan, D.T. Spreading Of Nanofluids Driven By The Structural Disjoining Pressure Gradient, 2004,Journal of Colloid and Interface Science, 2004, vol. 280, issue 1, s.192–201. DOI: 10.1016/j.jcis.2004.07.005.
47. McAndrew, J., Cisternas, P., Pruvot, A., Kong, X., Tong, S. Water Consumption and Proppant Transport Aspects of Foam Fracturing Fluids, **2017**, 1-8, SPE/AAPG/SEG Unconventional Resources Technology Conference, Austin, Texas, USA, DOI. https://doi.org/10.15530/URTEC-2017-2670102.
48. Wilk, K., Kasza, P., Czupski, M. Dodatki do spienionych płynów szczelinujących. *Przemysł chemiczny*, **2018**, 92/2, 1000-1005. DOI: 10.15199/62.2018.2.10.
49. Wilk, K., Kasza, P., Czupski, M. Dobór dodatków do energetyzowanych płynów szczelinujących. *Nafta-Gaz* **2016**, 12, 1092-1100. DOI: 10.18668/NG.2016.12.12.
50. Torabzadeh J., Langnes G.L., Robertson Jr. J. O., Yen T. F., Donaldson E. C., Chilingarian G. V., Yen T. F. (eds.): Enhanced Oil Recovery, II: Processes and Operations. *Elsevier Science Publishers* B. V. **1989**, 91-106.
51. AlYousef, Z., Almobarky, M., Schechter, D. Enhancing the Stability of Foam by the Use of Nanoparticles. *Energy Fuels*, **2017**, 31 (10), 10620–10627. DOI: 10.1021/acs.energyfuels. 7b01697.
52. Bjørnar, E. The Potential of Hydrophilic Silica Nanoparticles for EOR Purposes, *Petroleum Engineering and Applied Geophysics*, NTNU, Trondheim, Master thesis **2012,** 1-111.